

Cite this: *Green Chem.*, 2012, **14**, 1909

www.rsc.org/greenchem

PAPER

A structured catalyst based on cobalt phthalocyanine/calcined Mg–Al hydrotalcite film for the oxidation of mercaptan†

Zhiyong Sun, Lan Jin, Shan He, Yufei Zhao, Min Wei,* David G. Evans and Xue Duan

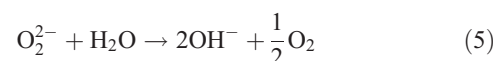
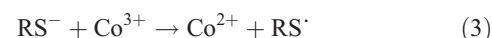
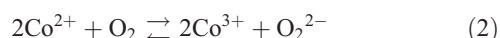
Received 15th November 2011, Accepted 12th April 2012

DOI: 10.1039/c2gc16462k

A structured catalyst has been fabricated by immobilizing cobalt phthalocyanine tetrasulfonate (CoPcS) on a mixed metal oxide (denoted as MMO) film, which exhibits excellent activity, stability and recyclability for mercaptan sweetening. Scanning electron microscopy (SEM) images show that the structured catalyst is composed of MMO nanoflakes whose *ab*-plane is perpendicular to the Al substrate, with desired mechanical strength and high adhesion to the substrate. In addition, *in situ* IR spectra and carbon dioxide temperature programmed desorption (CO₂-TPD) reveal that the moderate basic site is overwhelming in the CoPcS/MMO structured catalyst, while the strong basic site predominates in the corresponding CoPcS/MMO powder catalyst. It was found that the structured catalyst exhibits high conversion (85.7%) for the oxidation of mercaptan to disulphide, markedly higher than that of the corresponding powder catalyst (38.7%), as a result of the high exposure of active species as well as the synergistic effect between the oxidation center (CoPcS) and the moderate basic site. In addition, the structured catalyst shows superior catalysis-regeneration performance, which facilitates its repeatable and cyclic usage over a long period. Therefore, this work provides a facile and effective method for the fabrication of structured catalyst with high catalytic activity and stability, as well as recyclability, which can be used as an eco-friendly catalyst for the sweetening process in the petroleum refining industry.

1. Introduction

Mercaptans, which exist in petroleum products, including liquefied petroleum gas (LPG), naphtha, gasoline, kerosene, *etc.*, are highly undesirable since they have a foul odor, a highly corrosive nature, and lead to catalyst poisoning; it is therefore necessary to remove them from the petroleum products.¹ In the petroleum refining industry, the most commonly practiced method is the Merox process of sweetening, whose first step is to extract mercaptans from petroleum products with a caustic soda solution and then oxidize them to disulfides with air in the presence of cobalt phthalocyanine or its derivatives as catalysts.² The mechanism of this reaction which has been widely accepted is summarized in the following equations:³



However, the use of a great amount of caustic soda solution in this process leads to environmental and economic disadvantages in the refinery because its disposal is becoming more difficult and expensive due to the steady tightening of environmental regulations worldwide.⁴ Therefore, extensive studies have been conducted on substitution of caustic soda by solid bases so as to develop a more environmentally friendly and effluent-free process for mercaptan sweetening.

Mg–Al mixed metal oxides (denoted as MMOs) derived from the thermal decomposition of layered double hydroxide materials (LDHs),⁵ have been regarded as promising solid bases with controllable basicity *via* changing their chemical composition and thermal treatment parameters.⁶ Recently, it was reported that MgAl-MMO supported cobalt phthalocyanine (CoPc) catalysts, which include an oxidation site (Co²⁺) and basic site (MgAl-MMO) with cooperative interaction, can effectively oxidize mercaptans to disulfides.⁷ However, the CoPc/MMO powder catalysts generally suffer from deactivation, and their leaching as well as separation in catalytic process remain unresolved.

State Key Laboratory of Chemical Resource Engineering, Beijing University of Chemical Technology, Beijing 100029, China. E-mail: weimin@mail.buct.edu.cn; Fax: +86-10-64425385; Tel: +86-10-64412131

† Electronic supplementary information (ESI) available: Photograph (Fig. S1), SEM images (Fig. S2, Fig. S4–S6), XRD (Fig. S3 and S7). Chemical compositions (Tables S1 and S2). See DOI: 10.1039/c2gc16462k

A feasible solution to this problem is to develop structured catalysts in which a strong adhesion between catalyst and substrate can suppress the leaching of active species and facilitate recycle usage.

In recent years, extensive studies have been focused on the immobilization of LDH films or coatings on different substrates for the purpose of obtaining monolithic catalysts⁸ and adsorbents.⁹ Several ways have been reported for the fabrication of LDH films, including the dip-coating method,¹⁰ electrophoretic deposition,¹¹ solvent evaporation,¹² *in situ* growth¹³ and a layer-by-layer technique.¹⁴ For instance, Lü *et al.* reported that the film catalyst prepared by the calcination/rehydration process of a MgAl-LDH film showed high catalytic performance in the aldol condensation of acetone.⁸ MgAl hydrotalcite (HT) thin films prepared by the electrophoretic deposition (EPD) method can be used as selective adsorbents for heavy metal ions¹⁵ and CO₂.¹⁶ However, studies on MMO films as structured catalysts or adsorbents, to the best of our knowledge, are rather rare. Therefore, this inspired us to fabricate the structured catalyst, cobalt phthalocyanine supported on a MgAl-MMO film, for the oxidation of mercaptan. Compared with traditional powdered catalysts, the structured catalyst may possess the following advantages: (1) the effective combination of the active species (CoPc) and a high dispersion of MMO microcrystals is beneficial to increase the catalytic activity; (2) strong adhesion and mechanical stability of the structured architecture can significantly improve the manipulation and facilitate its regeneration.

In this work, we report the preparation of structured catalysts by supporting cobalt phthalocyanine tetrasulfonate (CoPcS) onto a mixed metal oxide (MMO) film resulting from calcination of LDH precursor, which was used for mercaptan sweetening process *via* the oxidation of 1-octanethiol to corresponding disulfide as a model reaction. The SEM image shows that the structured catalyst is composed of MMO nanoflakes with *ab*-plane perpendicular to the Al substrate. *In situ* IR spectra and CO₂-TPD demonstrate that three species of basic sites (weak, moderate and strong) exist on the surface of the CoPcS/MMO powder catalyst. In the contrast, moderate basic site predominates in the structured catalyst, which is a key factor for the catalytic reaction. The CoPcS/MMO structured catalyst exhibits much higher conversion, more stable regeneration and recyclability as well as convenient manipulation compared with the corresponding powder catalyst, owing to the high exposure of active species as well as the synergistic effect between the oxidation center (CoPcS) and the moderate basic site. By virtue of the incorporation of catalytic active species and moderate basicity of the immobilized MMO microcrystals, the CoPcS/MMO structured catalyst in this work can be prospectively applied as an eco-friendly catalyst for sweetening of oil in petroleum refining industry.

2. Experimental

2.1 Materials

Tetrasodium salt of cobalt(II) 4',4'',4''',4''''-tetrasulfophthalocyanine (Co(II)Pc(SO₃Na)₄, denoted as CoPcS) and 1-octanethiol (purity >97%) were provided by J&K Chemical Ltd. The pure aluminum substrate (purity >99.99%; thickness 0.2 mm) was purchased from Beijing General Research Institute for Non-Ferrous Metals. The following analytical grade chemicals were

used without further purification: ethanol, NaOH, (NH₂)₂CO, Mg(NO₃)₂·6H₂O. Deionized water was used in all the experimental processes.

2.2 Fabrication of the structured catalysts

The MgAl-LDH films were prepared by *in situ* crystallization on the pure aluminum substrate. The substrate was cleaned with acetone, ethanol and deionized water in sequence before use. In a typical procedure, 0.032 mol Mg(NO₃)₂·6H₂O and 0.194 mol (NH₂)₂CO were dissolved in deionized water to form a clear solution with a total volume of 600 ml. The Al substrate (28 cm × 15 cm) was rolled into tubular shape and immersed vertically in the solution, which was heated at 70 °C for 12, 24, 36 and 48 h, respectively. Afterwards, the substrate was withdrawn, rinsed with deionized water and dried at room temperature. The as-prepared MgAl-LDH film was heated at 500 °C for 4 h (heating rate: 2 °C min⁻¹), and then cooled to room temperature to obtain the MgAl-MMO film.

The structured catalysts, as shown in Fig. S1,† were prepared by immersing the fresh MMO film in an anhydrous methanol solution containing Co(II)Pc(SO₃Na)₄ of different concentrations (10, 20, 30, 40, and 50 ppm, respectively) with a dry N₂ flow at 25 °C for 1 h, followed by drying under vacuum at 50 °C for 2 h. The resulting structured catalysts (denoted as CoPcS/MMO-film) typically contain 0.68–1.52 mg CoPcS per 140 cm² aluminum substrate in this work. The catalysts of two comparison film samples, CoPcS/LDH-film and CoPcS/Al-film, were prepared by a similar procedure. Powder samples of CoPcS/LDH and CoPcS/MMO were prepared according to the reported method.¹⁷ Before use, all these catalyst samples were stored free of moisture and air.

2.3 Catalytic oxidation of mercaptan

The catalytic properties of the catalysts were tested in the oxidation reaction of 1-octanethiol, which was performed in a thermostatted double-walled glass flask equipped with a high-speed stirrer.^{17,18} The structured catalyst (with the substrate area of 140 cm²) containing 0.68–1.52 mg of CoPcS was rolled into a cylinder and placed into the reaction flask. After the injection of 1.40 ml of 1-octanethiol (containing 1000 ppm mercaptan sulfur in synthetic feed), the reaction occurred at 25 °C under constant oxygen pressure (1.0 atm). The catalytic behavior of powder catalysts containing the same content of CoPcS was evaluated under the same conditions. The reaction products were analyzed by GC-MS, and it was found that the disulfide (C₈H₁₇SSC₈H₁₇) was the only product, indicating a 100% of selectivity. No H₂O₂ accumulation was detected. Therefore, the conversion of 1-octanethiol proceeds according to the following equation: 4C₈H₁₇SH + O₂ → 2C₈H₁₇SSC₈H₁₇ + 2H₂O. The recycling test was performed by withdrawing the structured catalyst and then injecting new reactants.

2.4 Characterization

X-Ray diffraction (XRD) patterns of samples were obtained on a Shimadzu XRD-6000 diffractometer, using Cu Kα radiation

($\lambda = 0.154 \text{ nm}$) at 40 kV, 30 mA, a scanning rate of 5° min^{-1} , a step size of $0.02^\circ \text{ s}^{-1}$, and a 2θ angle ranging from 3 to 70° . The morphology and the thickness of the films were investigated by using a scanning electron microscope (Zeiss Supra 55) combined with energy dispersive X-ray spectroscopy (EDS) for the determination of metal composition. The accelerating voltage applied was 20 kV. All samples were sputtered with platinum. Transmission electron microscopy (TEM) images were obtained using a JEOL JEM-2100 transmission electron microscope. Elemental analyses for Mg, Al and Co were performed with a Shimadzu ICPS-7500 inductively coupled plasma spectroscopy (ICP) instrument on solutions prepared by dissolving the powders scraped from the films in dilute HNO_3 (1 : 1). Conversion was detected on Shimadzu 2010 GC-MS instrument using an HP5790 series mass selective detector with a silicone capillary column (DB-5, poly (5% diphenyl-95% dimethylsiloxane), $25 \text{ m} \times 0.2 \text{ mm}$, $0.33 \mu\text{m}$ film thickness). The specific surface area determination, pore volume, and size analysis were performed by BET and BJH methods using a Micromeritics ASAP 2020 analyzer. Prior to the measurements, samples were degassed at 200°C for 6 h.

The structure of CO_2 chemisorbed on hydrotalcite derived samples was determined by the Nicolet AVATAR 360 FT-IR spectrophotometer equipped with vacuum system and homemade transmission cell with ZnSe window. The activation of catalysts was carried out by heating to 500°C in muffle furnace for 4 h before measurement. The activated catalysts were heated to 500°C at high vacuum (10^{-4} Pa) for 1 h, and then cooled to room temperature. Data were recorded after CO_2 adsorption at room temperature and sequential evacuation at 50, 100, 150, 200, 250 and 300°C . Typically, 64 scans in the range of $4000\text{--}1000 \text{ cm}^{-1}$ were accumulated for each spectrum (resolution = 0.9 cm^{-1}). The absorbance scales were normalized to 20 mg pellets.

CO_2 -TPD of the catalysts was conducted on a TPDRO 110 series of Thermo. Before analysis, catalysts were heated to 500°C for 4 h in order to remove interference gases adsorbed on the catalysts surface. Catalysts (100 mg) were treated in N_2 at 500°C for 1 h and exposed to CO_2 stream at room temperature until a saturation coverage was obtained. Weakly adsorbed CO_2 was removed by flushing with He at 80°C for 0.5 h. The temperature was then increased at a linear rate of $5^\circ \text{C min}^{-1}$ from 50 to 500°C .

3. Results and discussion

3.1 Structural and morphological study of the structured catalyst

Fig. 1 illustrates the XRD patterns of the LDH film, MMO film, CoPcS/MMO film as well as the corresponding powder samples scraped from the film for comparison. For the LDH film (Fig. 1a), a rather weak reflection was observed at 2θ 35.1° , which can be attributed to the [012] reflection of the LDH phase; three strong reflections (marked with asterisk) appear originating from the Al substrate. The XRD pattern of the powder material scraped from the LDH film (Fig. 1d) shows a series of reflections at 11.7° , 23.5° , 61.0° and 62.5° , corresponding to the [003], [006], [110] and [113] reflections of an LDH phase, respectively.

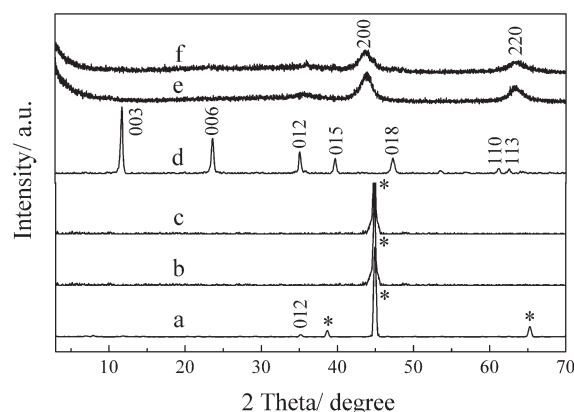


Fig. 1 XRD patterns of the (a) LDH film, (b) MMO film, (c) CoPcS/MMO film, (d) the LDH powder material scraped from the LDH film, (e) the MMO powder material scraped from the MMO film and (f) the CoPcS/MMO powder material scraped from the parent film. The asterisk symbol indicates reflections from the Al substrate.

Moreover, the basal spacing for the LDH material immobilized on Al substrate is $\sim 0.78 \text{ nm}$, close to the value reported for CO_3 -containing LDHs,¹⁹ which demonstrates the formation of an MgAl-LDH film on the Al substrate. The characteristic [012] reflection in Fig. 1a is indicative of a well-oriented assembly of LDH crystallites with their *ab* plane perpendicular to the substrate. In the case of the MMO film obtained by calcination of LDH film (Fig. 1b), only one reflection of the Al substrate was observed. However, the characteristic reflections [200] and [220] belonging to crystalline MgO phase²⁰ were detected for the powder material scraped from the MMO film (Fig. 1e), indicating the occurrence of phase transformation from LDH to MMO. After loading CoPcS onto the MMO film (Fig. 1c), no obvious change can be found; the scraped material (Fig. 1f) also displays the MgO reflections similar to Fig. 1e. Therefore, it can be concluded that an MgO phase was formed after calcination of the LDH film, and the subsequent loading of CoPcS did not change the structure of the MMO film.

The morphology of structured catalyst and its precursor revealed by SEM is shown in Fig. 2. Top-view and side-view of the LDH film (Fig. 2A and 2B) show uniform hexagonal plate-like microcrystals with diameter of 1.0–1.5 μm and thickness of 100–200 nm, whose *ab*-plane is perpendicular to the substrate. This is consistent with the XRD results in Fig. 1. Calcination of the LDH film leads to its transformation to MMO film, and the SEM images of the resulting product (Fig. 2C and 2D) show that it inherits the original hexagonal morphology of the LDH precursor with a little shrink in the size of hexagonal microcrystals (0.9–1.3 μm in diameter and 100–200 nm in thickness) compared with the parent LDH. Moreover, high dispersive MMO microcrystals interlaced with each other were observed, which is favorable to provide a high specific surface area. After loading CoPcS (Fig. 2E and 2F), no significant change in the morphology of CoPcS/MMO film was observed in comparison with the MMO film. The adhesion of the CoPcS/MMO film to the aluminum substrate was tested according to a reported method,²¹ and the result is shown in Fig. S2.† No significant peeling of the CoPcS/MMO layer was found after cross-cutting through the

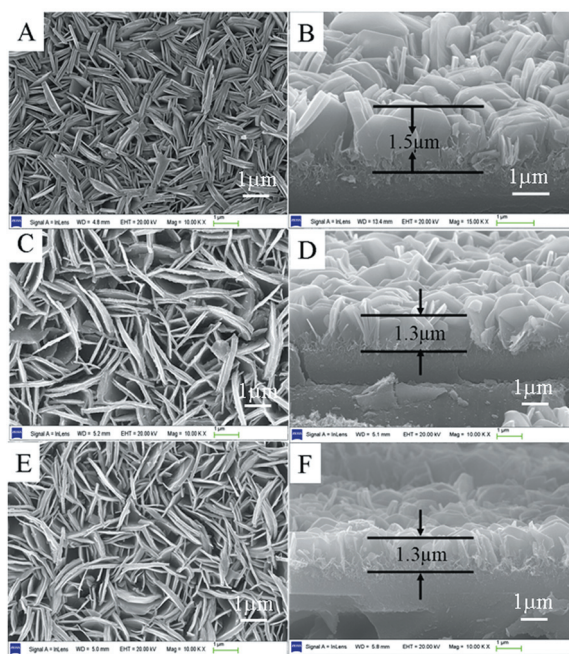


Fig. 2 SEM images for top-view and side-view of the LDH film (A, B), MMO film (C, D) and CoPcS/MMO film (E, F).

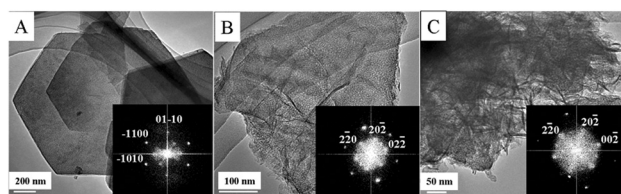


Fig. 3 TEM images of the (A) LDH, (B) MMO, and (C) CoPcS/MMO sample.

film, indicating a strong adhesion between the CoPcS/MMO film and the substrate.

The structure of the as-prepared LDH, MMO and CoPcS/MMO film was further investigated by TEM, which are shown in Fig. 3. Fig. 3A displays one piece of the hexagonal LDH platelet, and the corresponding SAED pattern (inset) exhibits hexagonally arranged bright spots, confirming its single-crystal nature of an LDH phase. Fig. 3B shows the TEM image of the MMO platelet, and the SAED pattern (inset) can be indexed as the [111] zone axis of a cubic MgO. Furthermore, it was found that the structure of the CoPcS/MMO (Fig. 3C) did not change compared with MMO, which is in accordance with the results of XRD and SEM.

3.2 Preparation of the structured catalysts for the oxidation of mercaptan

Influence of the LDH precursor. LDH films on aluminum substrates with different growth time ($t = 12, 24, 36$ and 48 h) were successfully prepared, which was confirmed by XRD (Fig. S3†). The signal intensity of characteristic reflection [012] increases gradually as the growth time of the LDH film

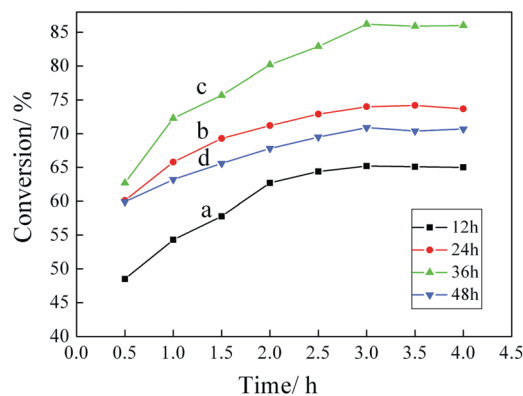


Fig. 4 Catalytic activity of the CoPcS/MMO- t structured catalysts for 1-octanethiol oxidation at room temperature and atmospheric pressure (a: $t = 12$ h; b: $t = 24$ h; c: $t = 36$ h; d: $t = 48$ h).

increases, and the [003] reflection appears after 48 h, indicating an enhancement in the LDH crystallinity. SEM images (Fig. S4†) display the morphology of the LDH films with different growth times (12–48 h) and their corresponding MMO films. It was found that the size of LDH microcrystals becomes larger and the stacking is more compact upon prolonging the growth time from 12 to 36 h (Fig. S4a–c†), while a decrease in size as well as serious aggregation of LDH microcrystals are observed as the time reaches 48 h (Fig. S4d†). Moreover, the corresponding MMO films show a similar change to the LDH films, which was confirmed by Fig. S4a₁–d₁†.

Structured catalysts were prepared by calcination of these LDH films mentioned above and then immersing them into a CoPcS methanol solution (30 ppm) for 1 h, which are represented as CoPcS/MMO- t (t denotes the growth time of LDH film precursor). Table S1† lists the corresponding chemical composition of these catalysts, from which it can be seen that both the content of magnesium and CoPcS increase with the increase of t . Catalytic activity evaluation of the CoPcS/MMO- t ($t = 12, 24, 36, 48$ h) structured catalysts for oxidation of mercaptan was performed, and the results are shown in Fig. 4. It can be seen that the activity of the structured catalyst increases at first to a maximum and then decreases along with the increase of crystallization time of LDH precursor. The CoPcS/MMO ($t = 36$ h, Fig. 4, curve c) film exhibits the highest conversion (85.7%) of mercaptan than other samples (Fig. 4, curves a, b and d). The results indicate that the size and stacking density of MMO microcrystals may impose influence on the specific surface area and pore size distribution of the structured catalyst, which will be discussed in the next section.

Influence of the loading amount of CoPcS. Structured catalysts represented as CoPcS/MMO- c (c stands for the concentration of CoPcS methanol solution) were prepared by immersing the MMO film into CoPcS methanol solution with different concentrations ($c = 10, 20, 30, 40$ and 50 ppm respectively) for 1 h. An increase in the CoPcS content of these catalysts along with the increase of concentration was found based on the results of elemental analysis (Table S2†), and their catalytic behavior for the oxidation of mercaptan is shown in Fig. 5. The conversion of mercaptan increases at first to a maximum

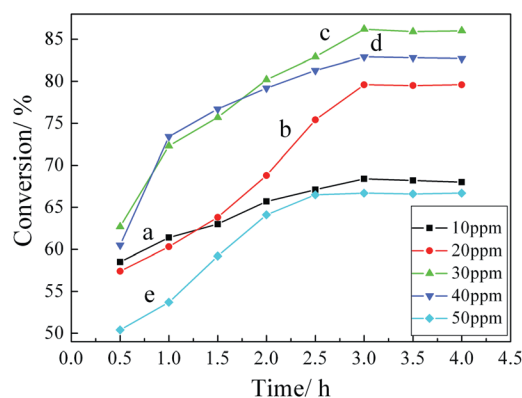


Fig. 5 Catalytic activity of the CoPcS/MMO-*c* structured catalysts for 1-octanethiol oxidation at room temperature and atmospheric pressure (a: *c* = 10 ppm; b: *c* = 20 ppm; c: *c* = 30 ppm; d: *c* = 40 ppm; e: *c* = 50 ppm).

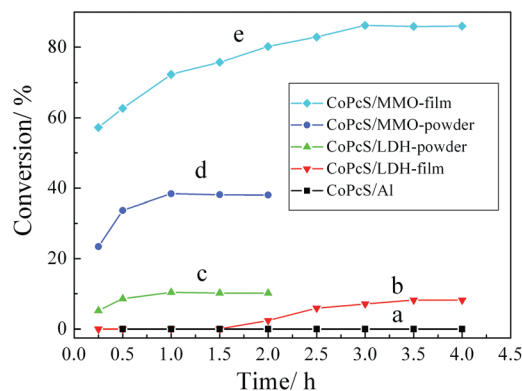


Fig. 6 Oxidation of mercaptan with the presence of various catalysts.

and then decreases as the concentration of CoPcS increases (Table S2†). The CoPcS/MMO catalyst (*c* = 30 ppm) displays the highest conversion (85.7%, curve c) among these structured catalysts. The gradual enhancement in the catalytic activity of CoPcS/MMO (*c* = 10, 20 and 30 ppm) is attributed to the increase of CoPcS content; while the decrease in the activity (*c* = 40 and 50 ppm) probably results from the aggregation of CoPcS. Therefore, it can be concluded that the architecture of support as well as the loading amount of CoPcS are key factors in determining the catalytic activity of the structured catalysts.

3.3 Catalytic oxidation of mercaptan with different catalysts

The catalytic performance of structured catalysts (CoPcS/MMO film) for the oxidation of mercaptan was studied, accompanied with the CoPcS/Al film, CoPcS/LDH film, CoPcS/LDH powder and CoPcS/MMO powder for comparison. The catalytic activity of these catalysts was tested (Fig. 6), and the results are listed in Table 1. No conversion was observed for the CoPcS/Al sample (Fig. 6a), indicating that Al substrate does not contribute to the reaction of mercaptan oxidation. The CoPcS/LDH catalysts (both film and powder) show rather low conversion levels, *i.e.*, 5.9% (Fig. 6b, film) and 10.2% (Fig. 6c, powder), owing to their weak basicity which will be discussed in the next section. In the

Table 1 Chemical composition, BET specific surface areas and conversion of mercaptan for various catalysts

Catalyst	Mg/Al ratio	Content of CoPcS (mg)	Content of MMO/LDH (mg)	S_{BET} ($\text{m}^2 \text{g}^{-1}$)	Conversion (%)
Al substrate		0.23			0.0
CoPcS/LDH-film ^a	2.13	1.20	36.6		5.9
CoPcS/LDH-powder	2.11	1.31	36.6	19.8	10.2
CoPcS/MMO-powder	2.11	1.12	32.9	269.2	38.7
CoPcS/MMO-film ^a	2.13	1.00	32.9		85.7

^a Area of the film catalyst: 140 cm^2 .

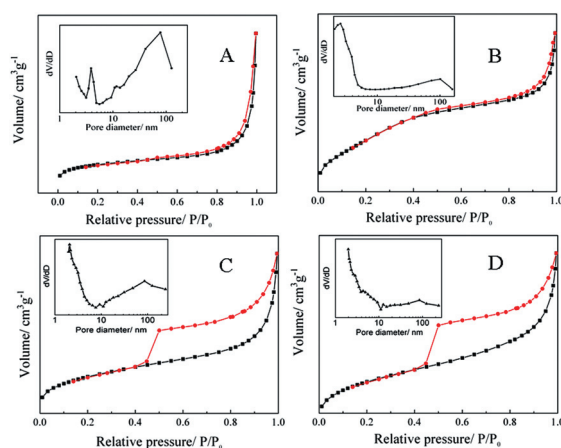
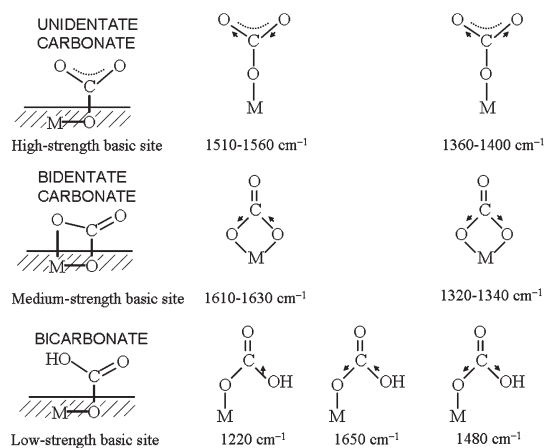


Fig. 7 Nitrogen adsorption-desorption isotherms and corresponding pore size distribution curves (inset) of (A) CoPcS/LDH-powder sample, (B) CoPcS/MMO-powder sample, (C) CoPcS/LDH-film, (D) CoPcS/MMO-film.

contrast, the CoPcS/MMO structured catalyst shows the highest conversion (85.7%, Fig. 6e), markedly superior to that of the corresponding CoPcS/MMO powder catalyst (38.7%, Fig. 6d). It was reported that both active species and basic site are necessary for the oxidation reaction of mercaptan.²² In this work, a synergistic effect between active CoPcS and basicity of MMO was observed based on the above results. In addition, for the CoPcS/MMO structured catalyst, a high dispersion of MMO microcrystals provides porous structure for the immobilization of CoPcS, which is beneficial to the diffusion and transfer of the reactant.

3.4 Sorption analysis of the structured catalysts

The nitrogen sorption measurements were performed to shed light on the textural and pore size distribution for the structured catalyst. Fig. 7 shows the N_2 adsorption-desorption isotherms and pore size distribution curves for the CoPcS/LDH-powder, CoPcS/MMO-powder, CoPcS/LDH-film and CoPcS/MMO-film respectively, and the specific surface area are summarized in Table 1. All these samples exhibit intermediate isotherm



Scheme 1 IR bands of adsorbed CO₂ surface species (Ref. 27a).

between type II (absence of a plateau at high p/p_0) and type IV adsorption (small N₂ adsorption at lower p/p_0) according to Groen's report.²³ An H3-type hysteresis loop without any limiting adsorption at higher p/p_0 was observed for the two powder samples, indicating the existence of macropores.²⁴ This is further confirmed by the corresponding wide distribution of pore size in the inset of Fig. 7A and 7B (4–120 nm; 3–160 nm), resulting from the aggregation of LDH or MMO particles.²⁵ In the case of the CoPcS/LDH and CoPcS/MMO film samples (Fig. 7C and 7D), an abrupt closure of the hysteresis loop at *ca.* $p/p_0 = 0.43$ was observed in the desorption isotherm. This phenomenon is indicative of the tensile strength effect (TSE),²³ which indicates the creation of mesopores <4 nm. However, taking into account the existence of TSE, the pore size distribution derived from the adsorption branch was applied for the film samples. A mixture of H2–H3 hysteresis loop was observed for the two film samples, indicating the presence of slit-shaped and maybe ink-bottle pores in the whole mesopore network.²³ The pore size distribution for the CoPcS/LDH and CoPcS/MMO film samples (2–120 nm) is attributed to the homogeneous morphology of LDH or MMO microcrystals and their oriented stacking on the substrate (Fig. S5†). As for the specific surface area however, the CoPcS/MMO material scraped from the substrate which retains its original morphology (Fig. S6†) shows a much lower value (15.5 m² g⁻¹) than that of the CoPcS/MMO powder sample (269.2 m² g⁻¹). The result indicates that the specific surface area of the catalyst is not a key factor in determining its activity, while the effective exposure of active sites is more crucial.

3.5 Alkaline effect of MMO

It is reported that basicity of catalysts is an essential factor in the catalytic oxidation of mercaptan.²⁶ Therefore, *in situ* FT-IR was applied to measure the basic site strength by analyzing the structure of CO₂ chemisorbed on basic sites of catalysts. It has been reported that three species of adsorbed CO₂ were detected, reflecting three different types of surface basic sites (Scheme 1).²⁷ Unidentate carbonates corresponding to strong basic sites exhibit a symmetric and asymmetric O–C–O stretching at 1360–1400 cm⁻¹ and 1510–1560 cm⁻¹ respectively; bidentate carbonates formed on moderate basic sites show symmetric

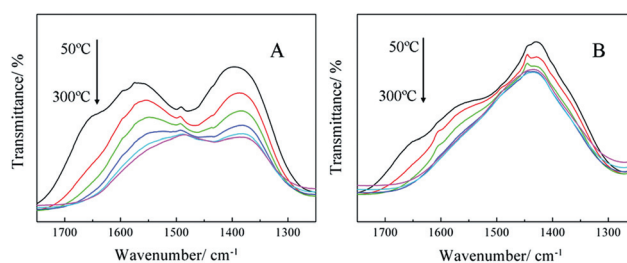


Fig. 8 *In situ* infrared spectra of CO₂ adsorbed on (A) CoPcS/MMO powder sample and (B) CoPcS/MMO film sample upon increasing evacuation temperature: 50 °C, 100 °C, 150 °C, 200 °C, 250 °C, 300 °C.

and asymmetric O–C–O stretching vibration at 1320–1340 cm⁻¹ and 1610–1630 cm⁻¹ respectively; bicarbonate species on weak basic sites on catalyst surface involve hydroxyl groups, displaying C–OH bending mode at 1220 cm⁻¹ as well as symmetric and asymmetric O–C–O stretching at 1480 and 1650 cm⁻¹, respectively.

In this work, Fig. 8 shows *in situ* infrared spectra obtained on the CoPcS/MMO powder and CoPcS/MMO film sample after CO₂ adsorption at 50 °C and sequential evacuation at 100, 150, 200, 250 and 300 °C. Three broad infrared bands were observed for the CoPcS/MMO powder sample (Fig. 8A) after the CO₂ adsorption at 50 °C, which are attributed to the superimposition of unidentate carbonates (1560–1510 cm⁻¹ and 1400–1360 cm⁻¹), bidentate carbonates (1630–1610 cm⁻¹ and 1340–1320 cm⁻¹) and bicarbonates (1650, 1480 and 1220 cm⁻¹). As the temperature increases to 100 °C, the intensity of two absorption bands attributed to unidentate and bidentate carbonates (1600–1500 cm⁻¹ and 1400–1300 cm⁻¹) decreases gradually and the band at 1650 cm⁻¹ assigned to bicarbonate species disappears. Upon further increasing temperature, the bidentate and unidentate carbonates disappear at 250 °C and 300 °C respectively. In the case of the CoPcS/MMO film sample (Fig. 8B), the inconspicuous band at 1650 cm⁻¹ owing to bicarbonate species was found at 50 °C, indicating the present of a few weak basic sites for the film sample; two relatively narrow absorption bands at 1600–1550 and 1450–1400 cm⁻¹ were observed, which are assigned to asymmetrical and symmetrical stretching vibration of bidentate carbonates, respectively. A strong and broad band at 1650–1300 cm⁻¹ is attributed to the remaining CO₃²⁻ species after the calcination of precursor LDH. The intensity of all these absorption bands decreases with the enhancement of temperature. As the temperature reaches to 200 °C, the bidentate carbonate species can be hardly detected. Therefore, it can be concluded that the CoPcS/MMO powder sample provides three kinds of basic sites – weak, moderate and strong; whereas few weak basic sites and predominant moderate basic sites exist in the CoPcS/MMO film catalyst.

The rate of CO₂ evolution as a function of sample temperature is shown in Fig. 9. The CO₂-TPD profile on the CoPcS/MMO powder sample (curve a) can be deconvoluted in three desorption peaks, reaching maximum desorption rate at ~100, 170 and 350 °C which are attributed to weak, moderate and strong basic site, respectively, in agreement with the results of *in situ* FT-IR (Fig. 8A). However, only one CO₂ desorption peak at 170 °C for the CoPcS/MMO film sample (curve b) was observed, indicating

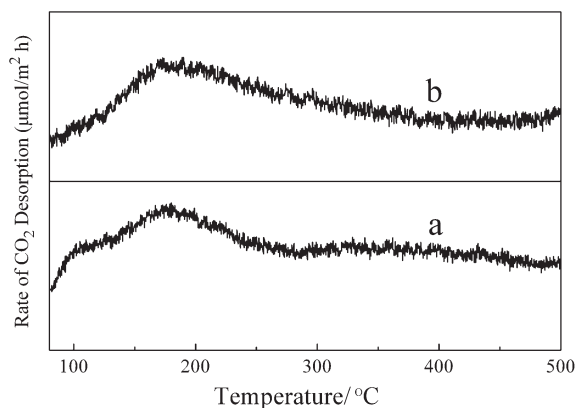


Fig. 9 TPD profiles of CO₂ on the (a) CoPcS/MMO powder sample and (b) CoPcS/MMO film sample.

the domination of moderate basic site. This is in approximately accordance with the results of *in situ* FT-IR (Fig. 8B). The percentage and number of CO₂ adsorbed on each basic site were calculated by integration, and the results are presented in Table S3.† Liu *et al.*¹⁷ reported that strong basic site leads to weaker adsorption and activation of mercaptan on the oxidation center of catalyst; while moderate basicity is favorable for the mercaptan oxidation. The moderate basic site on the surface of CoPcS/MMO powder sample accounts for 45.4% of the total basic sites; whereas the contribution of the moderate basic site is ~100% for the CoPcS/MMO film sample. In addition, the number of moderate basic sites for the CoPcS/MMO film is much larger than that of the CoPcS/MMO powder sample, accounting for the excellent catalytic activity of the structured catalyst.

The results above indicate that the oriented structure and high dispersion of MMO microcrystals result in the high exposure of moderate basic sites for the structured catalyst. A topotactic transformation from the hexagonal structure of LDH to the hexagonal MgO phase is believed to occur during the structural evolution of the LDH phase upon calcination. It has been reported that the moderate basic site is attributed to the Mg²⁺-O²⁻ pair with high coordination, while the strong basic site corresponds to O²⁻ ion with low coordination derived from the surface defects of MgO.²⁸ For the CoPcS/MMO powder sample, the existence of three kinds of basic sites is related to the formation of abundant defects during the phase transformation of LDH precursor particles. In the contrast, the high crystallinity of the LDH film leads to a low degree of surface defects of MgO phase during the structural evolution. This accounts for the domination of moderate basic site (Mg²⁺-O²⁻ pair) in the structured catalyst. In addition, the anchoring and orientation of MMO microcrystals effectively avoid their aggregation. As a result, it can be concluded that the synergistic effect between the moderate basic site and active species (CoPcS) in the structured catalyst plays a key role for its largely enhanced activity for the oxidation of mercaptan.

3.6 Recycling lifetime and regenerability of the structured catalyst

Since the recycling lifetime of catalysts is very essential for their practical application, the regeneration and recycle usage of the

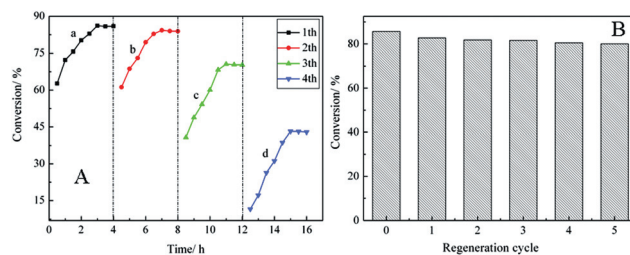


Fig. 10 (A) The catalytic capability of the CoPcS/MMO film catalyst for the oxidation of mercaptan. (B) Conversion of mercaptan vs. regeneration cycle.

structured catalyst were carried out. Fig. 10A shows the catalytic lifetime of structured catalyst performed with four cycles. It was found that the conversion of mercaptan decreased gradually (from 85.7% to 70.8%, Fig. 10A, curve a–c) in the first three cycles; obvious decrease in conversion (43.2%) was observed in the fourth cycle (Fig. 10A, curve d), indicating the inactivity of the structured catalyst. The regeneration of the structured catalyst was carried out by washing with acetone–dimethylsulfoxide solvent (1 : 1, v/v) followed by calcination (at 500 °C) and loading CoPcS. The consecutive catalysis-regeneration cycles of the structured catalyst were performed five times, and the results are shown in Fig. 10B. No significant decrease in the conversion of mercaptan was observed even in the fifth cycle. Moreover, the structure and morphology of the CoPcS/MMO film catalyst remained unchanged after five catalysis-regeneration cycles, which was revealed by XRD and SEM (Fig. S7†). In addition, the recycling lifetime and regeneration cycles of the powder catalyst were performed for comparison (Fig. S8†). A short recycling lifetime was observed (Fig. S8A†), and only 10.8% of conversion was maintained after the second regeneration cycle (Fig. S8B†), owing to the leaching of CoPcS as well as the aggregation of powder sample. Therefore, the results above indicate that the structured catalyst exhibits high catalytic activity, stability and regenerability, which is a promising catalyst for the sweetening process.

4. Conclusion

A structured catalyst based on a CoPcS supported MMO film was prepared, which shows high catalytic activity, high stability as well as good recyclability for the mercaptan sweetening process. The structured catalyst is composed of MMO nanoflakes whose *ab*-plane is perpendicular to the Al substrate, and its desired mechanical strength and high adhesion to the substrate were observed. In addition, the basicity and number of basic sites for catalysts were revealed by *in situ* IR spectra and CO₂-TPD, respectively. The results show that the powder catalyst provides three species of basic sites, *i.e.*, weak, moderate and strong basic site; while the moderate basic site is predominant in the structured catalyst. This is related to the reason that the structured catalyst is comprised of high crystalline MMO with less surface defects, resulting in the absence of a strong basic site. The structured catalyst CoPcS/MMO exhibits the highest conversion of mercaptan in comparison with other catalysts, which is attributed to the abundant moderate basic sites, high dispersion and

appropriate pore size distribution. More significantly, the synergistic effect between moderate basic site and oxidation center (CoPcS) plays a key role. The regeneration and recycle usage of the structured catalyst were also demonstrated. Therefore, the structured catalyst in this work exhibits the advantages of high catalytic activity and stability, good recyclability as well as convenient manipulation. It is expected that the CoPcS/MMO film can be potentially used as an eco-friendly catalyst for the sweetening process in oil refinery.

Acknowledgements

This work was supported by the 973 Program (grant no. 2011CBA00504), the National Natural Science Foundation of China, the 111 Project (grant no. B07004) and the Collaboration Project from the Beijing Education Committee.

Notes and references

- (a) B. Basu, S. Satapathy and A. K. Bhatnagar, *Catal. Rev. Sci. Eng.,* 1993, **35**, 571; (b) S. Bashkova, A. Bagreev and T. J. Bandoz, *Environ. Sci. Technol.*, 2002, **36**, 2777.
- G. Das, B. Sain, S. Kumar, M. O. Garg and G. MuraliDhar, *Catal. Today*, 2009, **141**, 152.
- T. Wallace, A. Schriesheim, H. Hurwitz and M. Glaster, *Ind. Eng. Chem. Process Des. Dev.*, 1964, **3**, 237.
- J. J. Alcaraz, B. J. Arena, R. D. Gillespie and J. S. Holmgren, *Catal. Today*, 1998, **43**, 89.
- (a) H. C. Greenwell, W. Jones, S. L. Rugen-Hankey, P. J. Hollimanc and R. L. Thompson, *Green Chem.*, 2010, **12**, 688; (b) A. M. Fogg, V. M. Green, H. G. Harvey and D. O'Hare, *Adv. Mater.*, 1999, **11**, 1466; (c) A. M. Fogg, J. S. Dunn, S. G. Shyu, D. R. Cary and D. O'Hare, *Chem. Mater.*, 1998, **10**, 351; (d) H. C. Greenwell, C. C. Marsden and W. Jones, *Green Chem.*, 2007, **9**, 1299.
- (a) A. L. McKenzie, C. T. Fishel and R. J. Davis, *J. Catal.*, 1992, **138**, 547; (b) D. Tichit, M. H. Lhouty, A. Buida, B. H. Chiche, F. Figueras, A. Auroux, D. Bartolini and E. Garrone, *J. Catal.*, 1995, **151**, 50; (c) S. Mitchell, T. Biswick, W. Jones, G. Williams and D. O'Hare, *Green Chem.*, 2007, **9**, 373; (d) B. M. Choudary, M. L. Kantam, C. V. Reddy, K. K. Rao and F. Figueras, *Green Chem.*, 1999, **1**, 187.
- (a) H. Liu, G. Ran, E. Min and X. Yang, *Chin. J. Mol. Catal.*, 1998, **12**, 221; (b) H. Liu, X. Yang, G. Ran and E. Min, *Acta Phys.-Chim. Sin.*, 1999, **15**, 918.
- Z. Lü, F. Z. Zhang, X. D. Lei, L. Yang, S. L. Xu and X. Duan, *Chem. Eng. Sci.*, 2008, **63**, 4055.
- X. L. Liu, M. Wei, D. G. Evans and X. Duan, *Chem. Eng. Sci.*, 2009, **64**, 2226.
- (a) E. Han, D. Shan, H. Xue and S. Cosnier, *Biomacromolecules*, 2007, **8**, 971; (b) J. H. Lee, S. W. Rhee and D. Y. Jung, *Chem. Commun.*, 2003, 2740.
- T. W. Kim, M. Sahimi and T. T. Tsotsis, *Ind. Eng. Chem. Res.*, 2008, **47**, 9127.
- J. Prince, A. Montoya, G. Ferrat and J. S. Valente, *Chem. Mater.*, 2009, **21**, 5826.
- T. Chen, S. L. Xu, F. Z. Zhang, D. G. Evans and X. Duan, *Chem. Eng. Sci.*, 2009, **64**, 4350.
- (a) L. Li, R. Z. Ma, Y. Ebina, K. Fukuda, K. Takada and T. Sasaki, *J. Am. Chem. Soc.*, 2007, **129**, 8000; (b) Z. P. Liu, R. Z. Ma, M. Osada, N. Iyi, Y. Ebina, K. Takada and T. Sasaki, *J. Am. Chem. Soc.*, 2006, **128**, 4872; (c) J. L. Gunjaker, T. W. Kim, H. N. Kim, I. Y. Kim and S. J. Hwang, *J. Am. Chem. Soc.*, 2011, **133**, 14998.
- S. He, Y. F. Zhao, M. Wei and X. Duan, *Ind. Eng. Chem. Res.*, 2011, **50**, 2800.
- T. W. Kim, M. Sahimi and T. T. Tsotsis, *Ind. Eng. Chem. Res.*, 2008, **47**, 9127.
- H. Liu and E. Min, *Green Chem.*, 2006, **8**, 657.
- J. H. Schutzen and J. Zwart, *J. Mol. Catal.*, 1979, **5**, 109.
- (a) J. H. Lee, S. W. Rhee and D. Y. Jung, *J. Am. Chem. Soc.*, 2007, **129**, 3522; (b) J. B. Han, J. Lu, M. Wei, Z. L. Wang and X. Duan, *Chem. Commun.*, 2008, 5188.
- S. Abelló, F. Medina, D. Tichit, J. Pérez-Ramírez, J. C. Groen, J. E. Sueiras, P. Salagre and Y. Cesteros, *Chem.-Eur. J.*, 2005, **11**, 728.
- D. E. Beving, A. M. P. McDonnell, W. S. Yang and Y. S. Yan, *J. Electrochem. Soc.*, 2006, **153**, 325.
- T. Buck, D. Woehle, G. S. Ekloff and A. Andreev, *J. Mol. Catal.*, 1991, **70**, 259.
- (a) J. C. Groen, L. A. A. Peffer and J. Pérez-Ramírez, *Microporous Mesoporous Mater.*, 2003, **60**, 1; (b) S. Abelló and J. Pérez-Ramírez, *Microporous Mesoporous Mater.*, 2006, **96**, 102.
- Y. F. Zhao, M. Wei, J. Lu, Z. L. Wang and X. Duan, *ACS Nano*, 2009, **3**, 4009.
- Y. Zhi, Y. G. Li, Q. H. Zhang and H. Z. Wang, *Langmuir*, 2010, **26**, 15546.
- H. Mei, M. Hu, H. X. Ma, H. Q. Yao and J. Shen, *Fuel Process. Technol.*, 2007, **88**, 343.
- (a) J. I. D. Cosimo, V. K. Diez, M. Xu, E. Iglesia and C. R. Apesteguía, *J. Catal.*, 1998, **178**, 499; (b) C. Morterra, G. Ghiotti, F. Boccuzzi and S. Coluccia, *J. Catal.*, 1978, **51**, 299; (c) R. Philipp and K. Fujimoto, *J. Phys. Chem.*, 1992, **96**, 9035; (d) J. I. Di Cosimo, C. R. Apesteguía, M. J. L. Ginés and E. Iglesia, *J. Catal.*, 2000, **190**, 261.
- (a) C. Chizallet, G. Costentin, M. Che, F. Delbecq and P. Sautet, *J. Phys. Chem. B*, 2006, **110**, 15878; (b) O. Cairon, E. Dumitriu and C. Guimon, *J. Phys. Chem. C*, 2007, **111**, 8015.